Thesis for the degree of Master of Science

Real-Time Parallel Optical Sampling

Tobias Eriksson

CHALMERS

Photonics Laboratory
Department of Microtechnology and Nanoscience
CHALMERS UNIVERSITY OF TECHNOLOGY
SE-412 96 Göteborg, Sweden 2011

Real-Time Parallel Optical Sampling
Tobias Eriksson

Photonics Laboratory
Department of Microtechnology and Nanoscience
Chalmers University of Technology
SE-412 96 Göteborg, Sweden
Telephone +46 (0)31 772 1000

Typeset using LaTeX

Cover: Illustrative example of the basic principe of parallel sampling, here with 4 branches.

Printed by Chalmers Reproservice
Göteborg, Sweden 2011

Abstract

Real-time parallel optical sampling shows great promise for overcoming the bandwidth limitation of fiber optical communication systems caused by the analog-to-digital converters in electronic sampling oscilloscopes. The basic concept of parallel optical sampling is to split the signal into multiple branches where the branches are delayed with equidistant sampling times. The signal branches are then sampled in the optical domain with a pulse of a few picoseconds and the branches are then detected in a standard fashion. The signal can then be reconstructed and transmission impairments can be compensated for using digital signal processing.

In this project, real-time parallel optical sampling with one sample per symbol synchronously sampled has been demonstrated for 25 Gbaud and 50 Gbaud QPSK signals. Since the bandwidth of the analog-to-digital converters used was 16 GHz, the sampling of 50 Gbaud QPSK signals that has been demonstrated is far beyond the capacity for traditional detection. The bit error rate performance at 10^{-3} for a back-to-back configuration was found to have a 2.8 dB penalty from the theoretical limit for 25 Gbaud QPSK signals and 2.6 dB penalty for 50 Gbaud QPSK signals. This penalty was most likely due to optical pulse imperfections such as amplitude noise. At 50 Gbaud the OSNR required for a bit error rate of 10^{-3} was roughly 15.4 dB.

Acknowledgement

First and foremost I would like to thank Ekawit Tipsuwannakul (Ek), for accepting to supervise me in this project. Without his support I would never have made it through the whole project. I can sincerely say that I have learnt more from the many hours spent with Ek in the lab than I could ever have learnt from any course. For the patience with all my questions, the many hours spent on introducing me to the lab, the pedagogy of his explanations and the guidance throughout the project, I am forever grateful.

I would also like to thank Prof. Peter Andrekson and Prof. Magnus Karlsson for having the faith in me and accepting me for this project as well as for their guidance throughout this project.

Further more, I would like to thank Pontus Johannisson for all the discussion regarding signal processing, general communication theory and the outline of certain parts of this thesis. I would also like to thank Mats Sköld who, even though he is not affiliated at Chalmers anymore, showed great interest in this project and could give some great tips and tricks in the lab as well as outside the lab. He gave me a good guidance, especially on the work with equalization using FIR filtering.

Moreover, Jianqiang Li, Martin Sjödin, Samuel Olsson and Henrik Sunnerud should have my thanks for various support during the project. I would also like to thank the rest of the photonics lab for creating such a nice working atmosphere and for helping me to a great start with invitations to various social events (such as playing football with the right to certain equipment at stake) and of course being superb lunch mates.

Last but not least, I would like to thank my partner Karin for her love, support and understanding with my sometimes long working days.

Tobias Eriksson

Göteborg
August 2011

List of Abbreviations

ADC	Analog to Digital Converter
ASK	Amplitude Shift Keying
BPSK	Binary Phase Shift Keying
CMA	Constant Modulus Algorithm
CW	Continuous Wave
DCF	Dispersion Compensating Fiber
DFB	Distributed Feedback (Laser)
EAM	Electro-Absorbtion Modulator
ECL	External Cavity Laser
EDFA	Erbium Doped Fiber Amplifier
FIR Filter	Finite Impulse Response Filter
FWHM	Full Width Half Maximum
GVD	Group Velocity Dispersion
HNLF	Highly Nonlinear Fiber
ISI	Inter-symbol interference
LO	Local Oscillator
MZ	Mach-Zehnder
MZM	Mach-Zehnder Modulator
NRZ	Non Return to Zero
OOK	On Off Keying
OSNR	Optical Signal to Noise Ratio

OTDM	Optical Time Division Multiplexing
PM	Phase Modulator
PRBS	Pseudo-Random Binary Sequence
PSK	Phase Shift Keying
QAM	Quadrature Amplitude Modulation
QPSK	Quadrature phase shift keying
RZ	Return to Zero
SMF	Single Mode Fiber
SNR	Signal to Noise Ratio
WDM	Wavelength Division Multiplexing/Multiplexed

Table of Contents

1. Introduction

The internet traffic is rapidly increasing and there is a demand for high bit rate services such as high definition video streaming. To meet the demand and to keep up with the increasing data traffic the capacity of today's communication systems has to be increased. The backbone of the internet is an architecture of fiber optical communication systems and this is where the demand for high bit rates is as strongest. There exists many methods to increase the bit rate of fiber optical communication systems such as wavelength division multiplexing (WDM), optical time division multiplexing (OTDM) and the use of advanced modulation formats.

The history of fiber optical communication essentially relies on two main inventions, the invention of the laser in 1960 [1] and the invention of the optical fiber, first proposed in 1966 [2] and realized in 1970 [3]. Due to these two inventions, it was possible to guide light over long distances. The first optical fibers had a quite high loss but much have happened since and today optical fibers with low loss can be fabricated. Loss as low as 0.16 dB/km at 1550 nm is commercial available today [4] but even as low as 0.15 dB/km has been demonstrated [5].

The third invention that has shaped the optical fiber communication systems to what they are today is the erbium doped fiber amplifier (EDFA) which was invented in the middle of the eighties [6]. The EDFA enabled amplification without transferring to the electrical domain and also a broad spectrum could be amplified which enabled WDM systems. Due to the EDFA high bandwidth optical communication systems could be constructed [7].

Traditionally, on off keying (OOK) has been the modulation format that has been dominating in fiber optical communication systems. There are two main reasons to why, where the first is the low complexity of the transmitter. A simple description of OOK would be that "light on" represents one bit and "light off" the other bit. The second reason is that all phase information is lost due to the square law detection of photo diodes thus using a modulation format which requires the phase information to be detected increases the complexity of the system [7, 8].

However, in recent years the use of more advanced modulation formats which can carry more than one bit per symbol has been the subject of a lot of research effort. Two modulation formats that are frequently used in fiber optical communication research are quadrature phase shift keying (QPSK) and

16 quadrature amplitude modulation (16-QAM). However to detect such formats, the phase has to be recovered which requires more advanced detection schemes. The two most common such detection schemes are differential detection [9] and coherent detection [10]. In this project coherent detection has been used.

For a real-time high-speed coherent receiver, the limiting factor for how high symbol rates that can be detected is the bandwidth of the analog to digital-converters (ADCs). The ADCs available in this lab are bandwidth limited at 16 GHz which is roughly what is used in many research laboratories. The top of the line ADCs have a bandwidth limit of 33 GHz, but is not yet commercial available [11].

To overcome this limitation, parallel optical sampling can be used which has been demonstrated in for instance [12] and [13]. The basic idea of parallel optical sampling is to split the signal into several branches and sample the signal in the optical domain with an optical pulse and then use several ADCs to sample each of the branches. The signal is then reconstructed using digital signal processing. Such a system is demonstrated and reviewed in this thesis.

1.1 Motivation

The current coherent receiver setup used in this laboratory is limited by the bandwidth of the ADCs on the real-time oscilloscope. The bandwidth of the ADCs is 16 GHz. Currently the receiver with highest real-time symbol rate that has been demonstrated in this laboratory was of 28 Gbaud, results are not yet published.

In this project the concept of parallel optical sampling is reviewed and demonstrated as a solution to overcome the bandwidth limitation of the ADCs. The overall aim of this project was to detect 50 Gbaud QPSK single polarization signals, synchronously sampled with one sample per symbol.

2. Introduction to Modulation Formats and Coherent Detection

In this chapter, a brief introduction to modulation formats and coherent detection will be presented.

2.1 Constellation Diagrams

The constellation diagram is a good tool for visualization of continuous signals and to provide an intuitive representation of different modulation formats. To explain the constellation diagram the signal space has to be defined. Consider a set of J orthogonal basis vectors $\{\Phi_1, \Phi_2, ..., \Phi_J\}$ and let the i:th transmitted signal $s_i(t)$ be represented by

$$\mathbf{s_i} = (s_{i1}, s_{i2}, ..., s_{iJ}), \qquad i = 1, 2, ..., M. \tag{2.1}$$

A total of M signals are sent and are expressed by

$$s_i(t) = \sum_{j=1}^{J} s_{ij}\Phi_j(t), \qquad i = 1, 2, ..., M. \tag{2.2}$$

In the majority of communication systems the most common signal space used consists of two basis vectors, here Φ_1 and Φ_2. An example of such a signal space is showed in figure 2.1 where the example signals s_1 and s_2 are represented [14].

For a fiber optical communication system, a modulated signal can generally be described as

$$s(t) = A(t)\cos(w_0 t + \theta(t)), \tag{2.3}$$

where $A(t)$ is the amplitude of the signal and $\theta(t)$ is the phase. ω_0 is the carrier frequency and is of much higher frequency than $A(t)$ and $\theta(t)$. This description of the signal is often called the *amplitude and phase description*. An equivalent description of the signal is

$$s(t) = I(t)\cos(\omega_0 t) - Q(t)\sin(\omega_0 t), \tag{2.4}$$

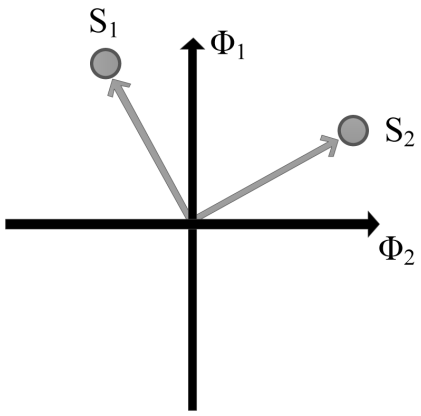

Figure 2.1: Constellation diagram showing two signal, s_1 and s_2, in the signal space spanned by Φ_1 and Φ_2.

where the relation to the *amplitude and phase description* is given by

$$I(t) = A(t)\cos(\theta(t)), \qquad Q(t) = A(t)\sin(\theta(t)) \tag{2.5}$$

where I(t) and Q(t) are called the *in-phase* and *quadrature* signals [14]. I and Q are orthogonal, due to the fact that the sine and cosine functions are orthogonal, and are therefore suitable basis vectors [15]. From here on the basis vectors seen in figure 2.1 will be used such as $\Phi_1 = I$ and $\Phi_2 = Q$.

It should be noted from equation 2.5 that phase and amplitude information is recovered from the I and Q expression as follows

$$\theta(t) = \arctan\left(\frac{Q(t)}{I(t)}\right), \tag{2.6}$$

$$A(t) = \sqrt{I^2(t) + Q^2(t)}. \tag{2.7}$$

2.2 Signal to Noise Ratio

If each symbol is considered to have an equal probability of being sent, the average signal energy is

$$E_\mathrm{s} = \frac{1}{M}\sum_{i=1}^{M} ||\mathbf{s}_i||^2, \tag{2.8}$$

where M is the number of constellation points and $\mathbf{s}_i$ is the i:th signal in the constellation diagram, as s_1 and s_2 in figure 2.1. If assumed that the noise of the channel is average white Gaussian noise with a power spectral density of $N_0/2$ the signal to noise ratio (SNR) is defined as

$$SNR = \frac{E_\mathrm{b}}{N_0}, \tag{2.9}$$

where E_b is the average signal energy per bit, related to E_s as $E_b = E_s/\log_2(M)$ [14, 16].

2.3 Modulation Formats

There exists many properties of an optical signal on which data can be modulated. The most intuitive such properties can be interpreted from equation 2.3, mainly the amplitude, phase and frequency of the signal. In optical communication the polarization can also be used to carry data [17, 10]. The frequency is not commonly modulated in fiber optical communication systems due to the fact that WDM systems with narrow channel spacings are often desired and that the realization of a receiver that is able to detect frequency modulated optical signals is of high complexity. Furthermore, a stable frequency is desired if a coherent detection scheme is to be used [8].

Traditionally in fiber optical communication systems, only the amplitude has been used to carry data but in recent years the use of the phase and the polarization have become much more widely used [10].

2.3.1 On Off Keying and Amplitude Shift Keying

OOK is the modulation format that traditionally has been most widely used in fiber optical communication system and is also the modulation format that is dominating in commercial systems. This is mostly due to the fact that it is the most simple modulation format possible and the fact that the square law of optical detectors makes it impossible to directly detect the phase of the signal. With OOK the data is modulated in a binary fashion such that "light on" represents one bit and "light off" the other bit [17, 10]. An advantage of using OOK over other modulation formats is that both the receiver and transmitter structures can be constructed with very low complexity. However, the most prominent drawback is that each symbol only carries one bit. The constellation diagram for OOK can be seen in figure 2.2.

For amplitude shift keying (ASK) it is, as the name implies, the amplitude that is modulated so that different intensities represent different symbols. OOK is the most simple form of amplitude shift keying and more advanced amplitude shift keying formats would have more signal states along the positive I-axis in figure 2.2 [18].

2.3.2 Phase Shift Keying

For phase-shift keying (PSK) the information is modulated onto the phase of the carrier. The most simple form of PSK is binary PSK (BPSK) of which the constellation diagram can be seen in figure 2.3(a). BPSK carries one bit per symbol, the same as OOK. However, as can be seen from the constellation

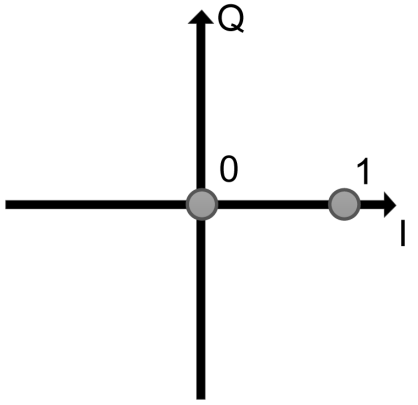

Figure 2.2: Constellation diagram for OOK.

diagrams in figure 2.3(a) and figure 2.2, BPSK require only half of the average signal energy compared to OOK for the same SNR.

Quadrature phase-shift keying, QPSK, is a modulation format on which excessive research has been conducted for fiber optical communication [10]. For QPSK four constellation points are used, as seen in figure 2.3(b), which enables each symbol to carry two bits [18]. QPSK can also be seen as two independent BPSK channels which is also a common way to implement a QPSK transmitter where two independent BPSK modulators are used with a relative phase shift of 90° [19].

This can of course be extended so that more constellation points are used. The next step after QPSK would be 8PSK for which the constellation diagram is seen in figure 2.3(c). As seen, 8PSK can carry 3 bits per symbol [18]. 8PSK is however far from being as excessively used in research as QPSK, however transmission over long links of fiber using 8PSK has been demonstrated in for instance [20].

It is of course possible to go to even higher number of constellation points but the spacing between the constellation points will be very small increasing the probability of error, therefore other modulation formats are often considered for higher order of bits per symbol.

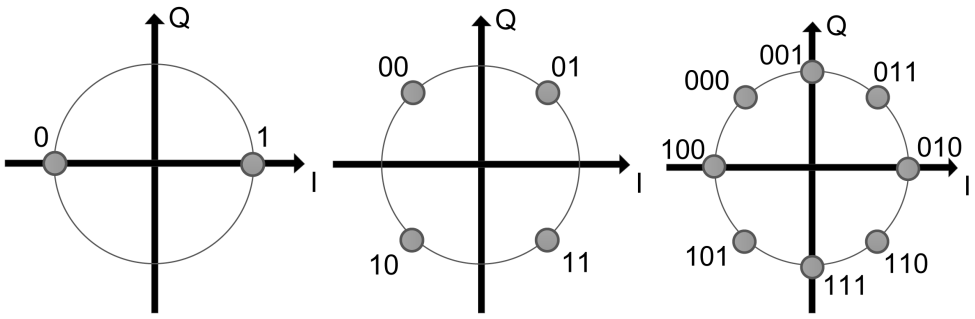

(a) BPSK (b) QPSK (c) 8PSK

Figure 2.3: Constellation plots for different levels of phase-shift keying.

2.3.3 Quadrature Amplitude Modulation

Quadrate Amplitude Modulation (QAM) is basically a combination between ASK and PSK such that both the amplitude and phase information is used to carry data. 16-QAM has been subject of excessive research in the last few years and is together with QPSK one of the most reviewed advanced modulation format in fiber optical communication[10].

The constellation diagram for 16-QAM can be seen in figure 2.4, each symbol can carry 4 bits. Note that when 16-QAM is mentioned it most often refers to the rectangular form that is seen in figure 2.4, however any placement of the 16 constellation points are of course possible. In fiber optical communication the rectangular format is most common but in wireless and electrical communication other non-rectangular 16-QAM formats are common such as V.29 modem standard and the double circle 16-QAM [17].

Higher order of modulation is of course possible and is often denoted M-QAM where M is the number of constellation points. 32-QAM has been been demonstrated over long fiber links [21] as well as 64-QAM [22]. 128-QAM has also been demonstrated in research setups [23] as well as 256-QAM [24] and even 512-QAM has been demonstrated over a single fiber link [25]. However it should be noted that these high order modulation formats are quite rarely used compared to 16-QAM and QPSK.

2.4 Coherent Detection

When modulation formats which uses phase information to carry data is considered, a more sophisticated receiver architecture has to be designed. This is due to the fact that in a standard photodiode all phase information is lost due to the square law detection [7]. Today, the two most widely used of such techniques are differential detection [9] and coherent detection [10], where coherent detection has been used in this project. Coherent detection and differential detection have different advantages and disadvantages which can be reviewed from different aspects. A brief summary would be that coherent detection has

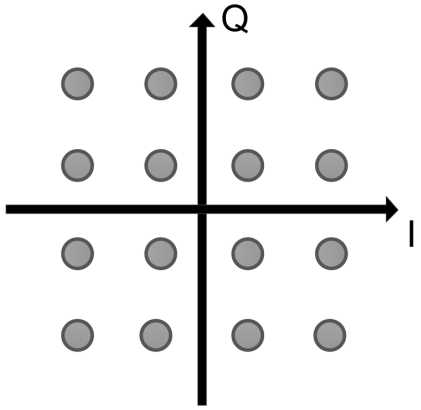

Figure 2.4: Constellation diagram for 16-QAM.

a greater sensitivity and since it is the E-field that is detected, compensation for transmission impairments can be performed with digital signal processing. Differential detection on the other hand can be implemented with a much less complex receiver structure thus providing low-cost solutions. Also, due to the differential encoding, differential detection is not limited by the ADC bandwidth in the same way as coherent detection [9]. Here a short introduction to coherent detection will be given, for a more profound review see for example [26], [10] or [27].

Coherent receivers were a big research topic in the eighties. Back then the focus of the research was the improved receiver sensitivity that could be achieved for direct detection of OOK [10]. However, the research was stalled when the EDFA was introduced and high sensitivity could be achieved without using coherent detection techniques [28]. In the last few years, when a lot of research has been devoted to increasing the spectral efficiency by using advanced modulation formats such as QPSK and 16-QAM which requires the phase information to be recovered, coherent detection has become a hot research topic again [10].

A coherent optical receiver can be implemented in a number of ways with the resemblance that the received signal is mixed with a local oscillator (LO) as a phase reference as seen in figure 2.5 [10]. The received signal can be described as

$$E_{\mathrm{s}}(t) = A_{\mathrm{s}}(t)\exp(j\omega_{\mathrm{s}}t), \tag{2.10}$$

where $A_s(t)$ is the complex amplitude and ω_s is the angular frequency. The signal from the local oscillator is given by

$$E_{\mathrm{LO}}(t) = A_{\mathrm{LO}}\exp(j\omega_{\mathrm{LO}}t). \tag{2.11}$$

Balanced detection is generally introduced as shown in figure 2.5. The reason that balanced detection most often is used is that it can suppress the intensity noise from the LO [29]. The coupler is constructed such that a 180° phase

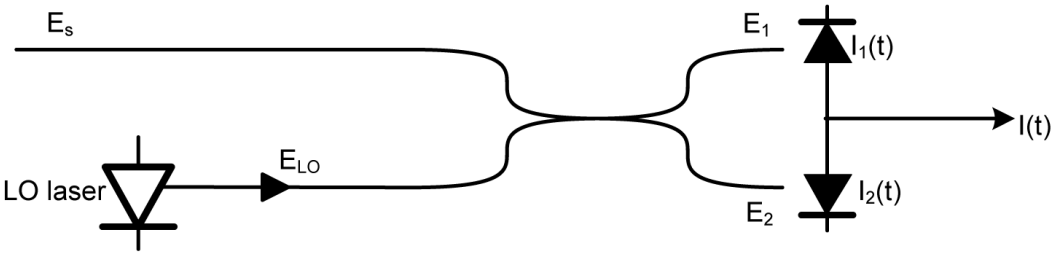

Figure 2.5: Schematics for a coherent receiver with balanced detection.

shift is induced to either the received signal or the LO on one of the output ports. The signals incident to the two photo diodes can then be expressed as

$$E_1 = \frac{1}{\sqrt{2}}(E_\mathrm{s} + jE_\mathrm{LO}), \tag{2.12}$$

$$E_2 = \frac{1}{\sqrt{2}}(jE_\mathrm{s} + E_\mathrm{LO}). \tag{2.13}$$

The electrical currents out from the photo diodes, both assumed to have a responsivity of $\mathfrak{R}$, are then given by

$$I_1(t) = \frac{\mathfrak{R}}{2}[P_\mathrm{s} + P_\mathrm{LO} + 2\sqrt{P_\mathrm{s}P_\mathrm{LO}}\sin(\omega_\mathrm{IF}t + \theta_\mathrm{sig}(t) + \theta_\mathrm{LO}(t) + \theta_\mathrm{n}(t))], \tag{2.14}$$

$$I_2(t) = \frac{\mathfrak{R}}{2}[P_\mathrm{s} + P_\mathrm{LO} - 2\sqrt{P_\mathrm{s}P_\mathrm{LO}}\sin(\omega_\mathrm{IF}t + \theta_\mathrm{sig}(t) + \theta_\mathrm{LO}(t) + \theta_\mathrm{n}(t))], \tag{2.15}$$

where ω_IF denotes the intermediate frequency and is given by $\omega_\mathrm{IF} = \omega_\mathrm{s} - \omega_\mathrm{LO}$. $\theta_\mathrm{sig}(t)$ and $\theta_\mathrm{LO}(t)$ denotes the phase of the received signal and the LO respectively and $\theta_\mathrm{n}(t)$ denotes the overall laser phase noise. Finally, the output of the balanced detector can then be expressed as

$$\begin{aligned} I(t) &= I_1(t) - I_2(t) \\ &= 2\mathfrak{R}\sqrt{P_\mathrm{s}(t)P_\mathrm{LO}}\sin(\omega_\mathrm{IF}t + \theta_\mathrm{sig}(t) - \theta_\mathrm{LO}(t) + \theta_\mathrm{n}(t)), \end{aligned} \tag{2.16}$$

where to power from the LO, P_LO can be assumed to be constant and $\theta_\mathrm{LO}(t)$ only accounts for the phase noise that varies with time [26, 27, 7]. As seen from equation 2.16, both the phase and the amplitude information can be retrieved.

2.4.1 The 90° Optical Hybrid

The receiver shown in figure 2.5 can only detect one of the phase components. To achieve phase diversity a more advanced architecture is required. The most common way to achieve phase diversity is to use a 90° optical hybrid setup for which the schematics is shown in figure 2.6. The optical hybrid is constructed

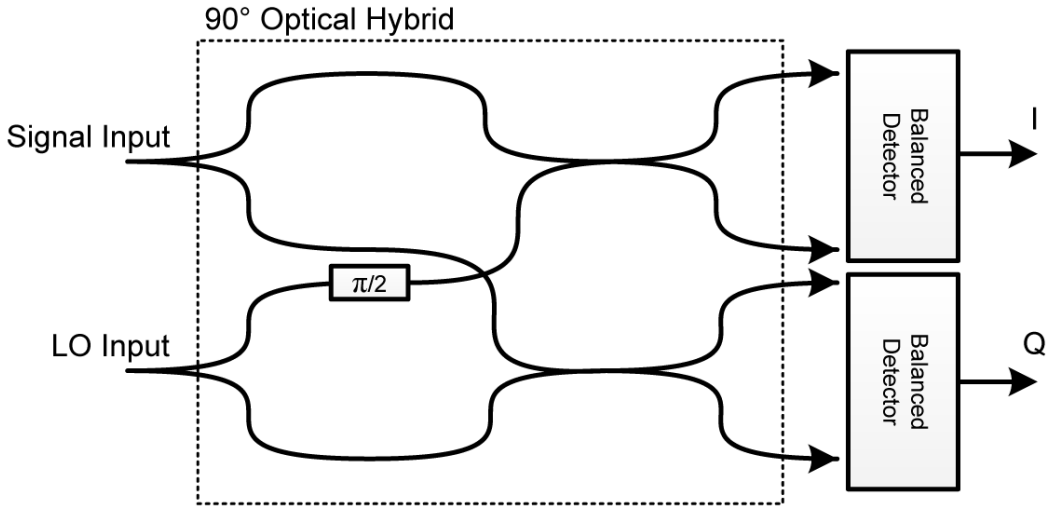

Figure 2.6: Schematics for a 90° optical hybrid.

such that LO has a 90° relative phase shift when interacting with the signal at the couplers as seen in figure 2.6. The optical hybrid is often followed by two balanced detectors, with the same concept as in figure 2.5. The output from the balanced detectors is given as

$$I(t) = 2|E_{\mathrm{s}}(t)||E_{\mathrm{LO}}|\cos(\omega_{\mathrm{IF}}t + \theta_{\mathrm{sig}}(t) + \theta_{\mathrm{LO}}(t) + \theta_{\mathrm{n}}(t)), \tag{2.17}$$

$$Q(t) = 2|E_{\mathrm{s}}(t)||E_{\mathrm{LO}}|\sin(\omega_{\mathrm{IF}}t + \theta_{\mathrm{sig}}(t) + \theta_{\mathrm{LO}}(t) + \theta_{\mathrm{n}}(t)), \tag{2.18}$$

where $E_{\mathrm{s}}(t)$ is the received optical field and E_{LO} is the optical field of the LO. θ_{sig} and θ_{LO} are the phases of the received and the LO respectively. $\theta_{\mathrm{n}}(t)$ denotes the overall laser phase noise. Hence, the I and Q information of a signal modulated by, for example QPSK or 16-QAM, can be recovered using a 90° optical hybrid [26, 7, 10].

3. Pulse Source

Pulse sources with high repetition rate and high quality has many applications in optical communication systems such as OTDM and, as in this project, optical sampling. There exists many methods to achieve picosecond pulses, all with different advantages and drawbacks, of which the most common will be briefly introduced here.

Temporal compression due to self phase modulation in a highly nonlinear fiber (HNLF) followed by further compression and amplification in a fiber optical parametric amplifier of pulses generated by a Mach-Zehnder modulator (MZM) shows great results [30]. This method can generate pedestal free 1.2 ps pulses with a repetition rate of 40GHz with great extinction ratio but the setup is of high complexity [30].

A much more simple technique is to use a continuous wave (CW) laser and drive an electro-absorbtion modulator (EAM) as a pulse carver which has been shown capable of generating 10 ps pulses at a repetition rate of 28 GHz [31] but shorter pulses is hard to achieve with this technique [32].

A common method to generate picosecond pulses is to use an actively mode-locked fiber laser [33, 34], although the base repetition rate of this technique is usually only 10 GHz [35]. Several methods can be used to increase the repetition rate to for example 20 GHz [36] or 40Ghz [35] but this will increase the complexity of the system drastically [32]. Two main drawbacks with a mode-locked fiber laser are that it is complicated to achieve long-time stability and that it is difficult to tune the repetition rate [37].

Another widely used method to create picosecond pulses is to induce a high chirp to a pulse train and then achieve pulse compression by propagation through a dispersive medium such as dispersion compensating fiber (DCF) [38], a chirped fiber Bragg grating [39] or standard single mode fiber (SMF) [40]. The basic idea of this method can be understood from figure 3.1, where it can be seen that for a Gaussian pulse with a certain initial chirp and initial width there exists a point when the pulse is propagated through a dispersive medium where the pulse is maximally compressed. There exists several similar methods to achieve highly chirped pulses where most setups utilizes a phase modulator (PM) to induce the high chirp. A directly modulated laser followed by phase modulation is shown in [38], a CW laser followed by a MZM and PM is shown in [41]. An alternative method is presented in [42] where a MZM followed by an optical bandpass filter is utilized to create highly chirped pulses.

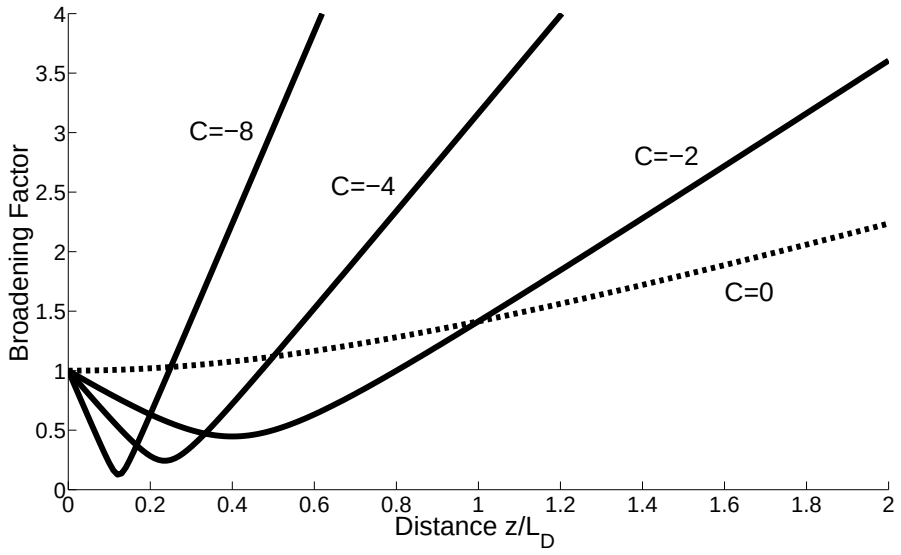

Figure 3.1: Broadening factor for linearly chirped Gaussian pluses.

3.1 Desired Characteristics of Sampling Pulses

As discussed, there exists many methods to achieve picosecond pulses and each method brings different features and problems. To characterize the pulses and to get a measure on how well suited the pulses are for an optical sampling systems the following characteristics can be determined.

The full-width half-maximum (FWHM) of the pulses has to be sufficiently small, a few to 10 ps is a common requirement for optical sampling systems [43, 33, 41]. Ideally the pulses should be chirp free at the point where the pulses are interacting with the sampled signal. Further, the pulses should ideally be pedestal free since pedestal will cause inter-symbol interference (ISI) [33]. Also, a high SNR and a high pulse extinction ratio is required [30].

3.2 Implemented Pulse Source

For this project, the implemented pulse source was similar to what was done by Sköld *et al.* in [44]. The pulse source was constructed for two pulse repetition rates, namely 12.5 GHz and 25 GHz. The schematics of the setup can be seen in figure 3.2, where solid and dashed lines represents optical domain and electrical domain respectively. The MZM is used to carve out pulses whereas the phase modulator is used to induce chirp on the pulses. The amount of chirp induced can be controlled by the electrical amplifier to the phase modulator. The basic idea behind this setup can be understood from the following equation

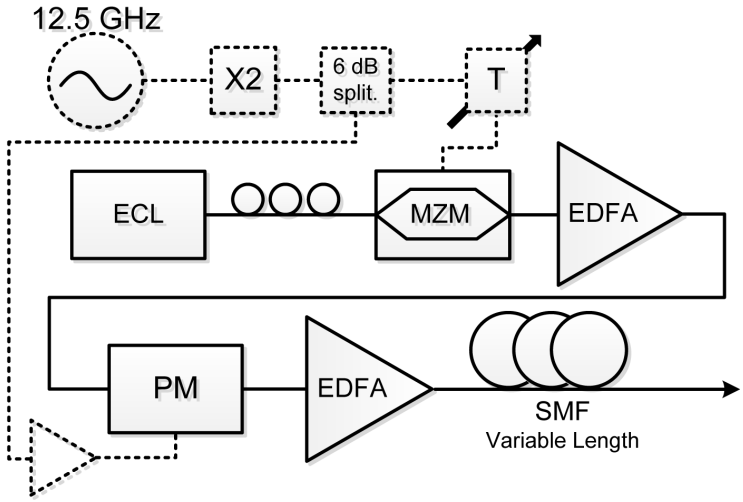

Figure 3.2: Setup of the first pulse source, dashed lines indicate components in electrical domain. Note that attenuators used are not shown.

$$b_f(z) = \frac{T_1(z)}{T_0} = \left[\left(1 + \frac{C\beta_2 z}{T_0^2}\right)^2 + \left(\frac{\beta_2 z}{T_0^2}\right)^2\right]^{\frac{1}{2}}, \tag{3.1}$$

where T_0 is the original pulse width and $T_1(z)$ is the width of the pulses, with initial chirp C, at position z in a dispersive medium with a certain group velocity dispersion (GVD) parameter β_2 [45].

Equation 3.1 is plotted in figure 3.1 and it can be seen that by propagating chirped pulses in a dispersive medium a compression of the pulse width can be achieved. It is also seen that for a fixed chirp there exists a length which gives a minimum pulse width, here the pulse is said to be transform limited (chirp free). For the first pulse source constructed in this project, the dispersive medium used was standard SMF and the length of the SMF could be varied in steps of 100 m. With the experimental setup used in this project and 12.5 GHz pulse repetition rate the length of SMF needed to get close to a transform limited pulse was typically in the range of 3000 to 4000 m whereas with 25 GHz repetition rate, a much higher chirp could be induced reducing the length of SMF needed to typically close to 1000 m.

Figure 3.3 shows the pulse width as a function of fiber length for the pulse source operating at 25 GHz repetition rate. As seen the minimum pulse width for this setup could be achieved at 800 m, however the pulse was more symmetrical and had less pedestal at 1000 m. The difference in pulse width at this point compared to the minimum was only 0.1 ps.

However it was found that the original pulse source was not optimized for sampling 50 GHz QPSK data and some modifications to the original pulse source had to be made which can be seen in figure 3.4. As seen, a second MZM

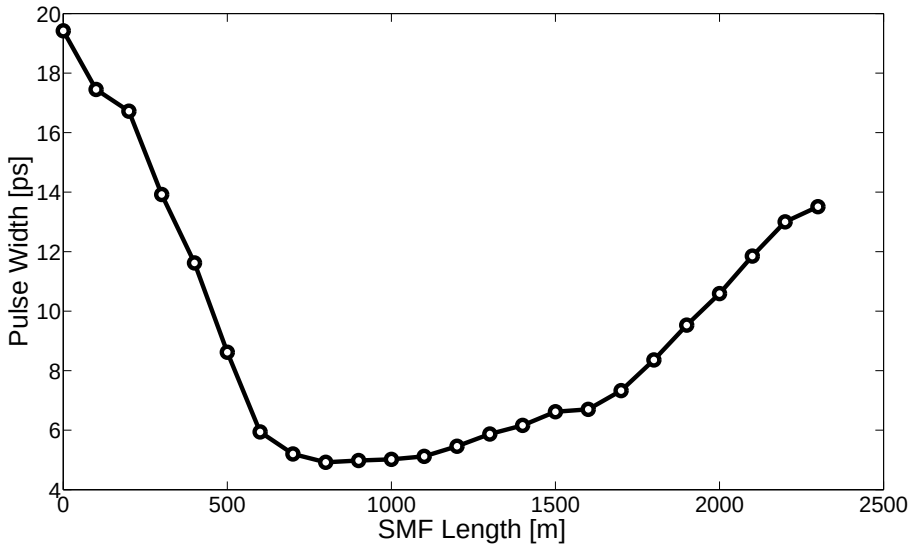

Figure 3.3: Pulse width as a function of fiber length for the first pulse system with 25 GHz repetition rate.

was implemented, mainly to reduce pedestal and increase the extinction ratio. DCF was mainly used as dispersive medium followed by SMF, this reduced the total length of fiber needed due to the fact that the DCF had a much higher GVD parameter, roughly 10 times, than the SMF. The shorter total fiber length should reduce timing jitter and temporal drifts. An attenuator before the electrical amplifier to the phase modulator was varied so that the pulse width after propagation was roughly 8 ps.

The output from the pulse source can be seen in figure 3.5. The pulse width was found to be 8.4 ps, the duty cycle was 21 %, the amplitude SNR was 31 dB and the extinction ratio was 24.4 dB. These measurements was done using an optical sampling oscilloscope with 1 ps resolution.

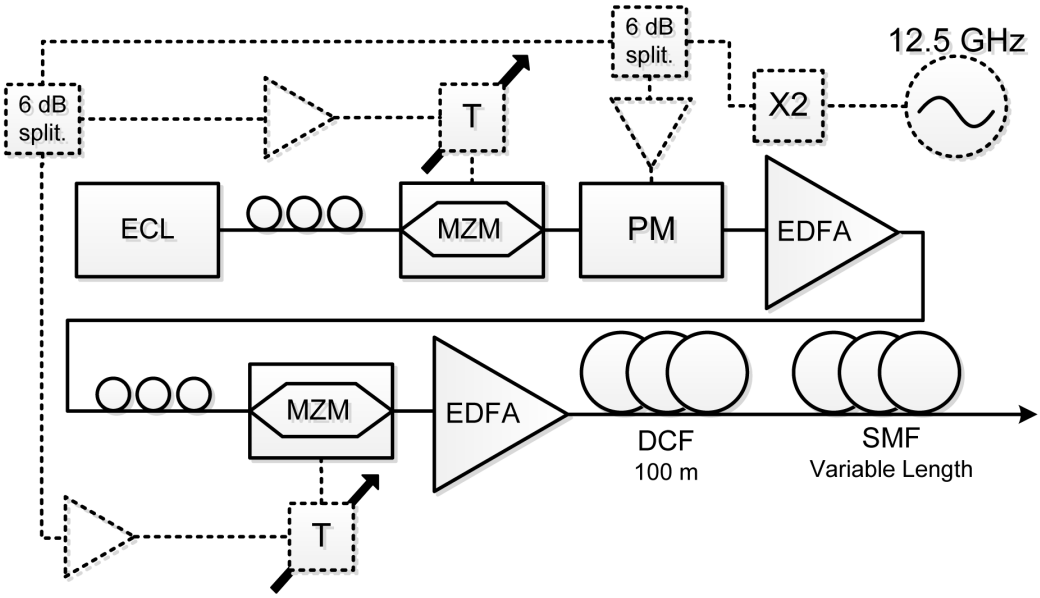

Figure 3.4: Setup of the final pulse source, dashed lines indicate components in electrical domain. Note that the electrical attenuators used are not shown.

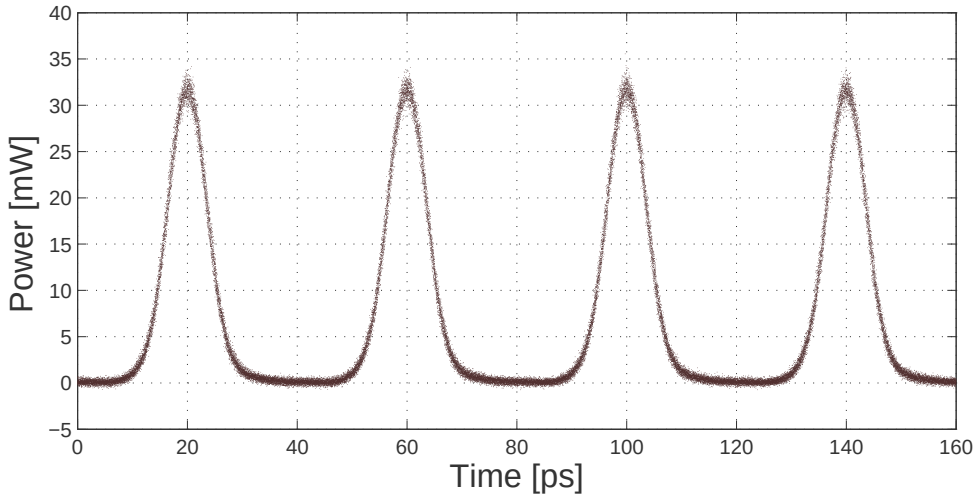

Figure 3.5: Pulse shape for the final pulse source. The FWHM pulse width is 8.4 ps.

4. Parallel Optical Sampling System

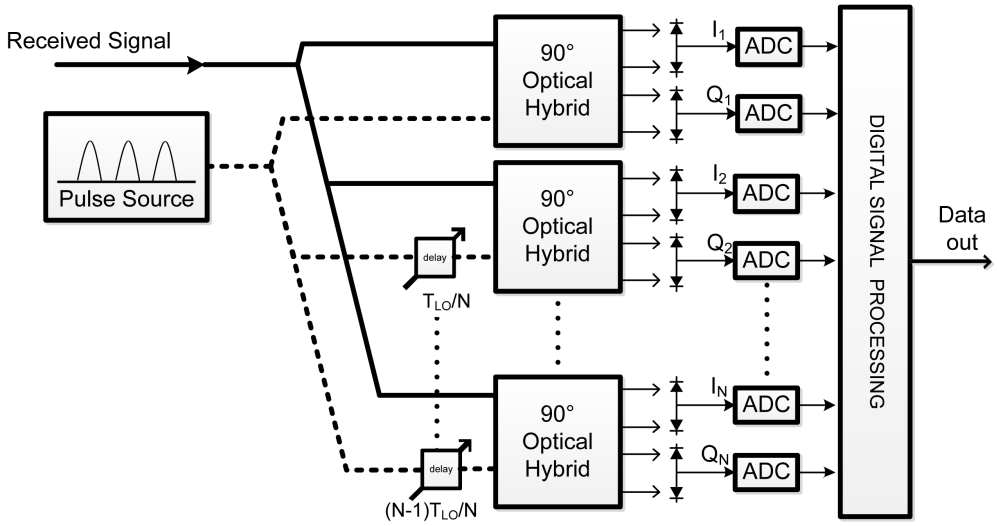

Figure 4.1: Schematics for the basic principle of parallel optical sampling

The basic idea of parallel optical sampling can be seen in figure 4.1 where N parallel optical samplers are shown. Note that it is assumed that the electrical samplers are optimized so that the sampling occurs at the pulse maximum. The pulsed local oscillator and the received signal are split into N branches. The pulse train of the i:th branch is delayed by

$$\tau_i = \frac{(i-1)T_{\mathrm{LO}}}{N}, \tag{4.1}$$

where $T_{\mathrm{LO}} = 1/R_{\mathrm{LO}}$ is the time period between the pulses and R_{LO} is the repetition rate of the pulses. If the pulses are delayed in this fashion, the optical sampling events are equidistant. Figure 4.2 shows the alignment in time for an optical sampling system using N = 4. The photocurrents I_{n} and Q_{n} after the balanced detectors are sampled using ADCs as seen in Figure 4.1. The ADC sampling is done at

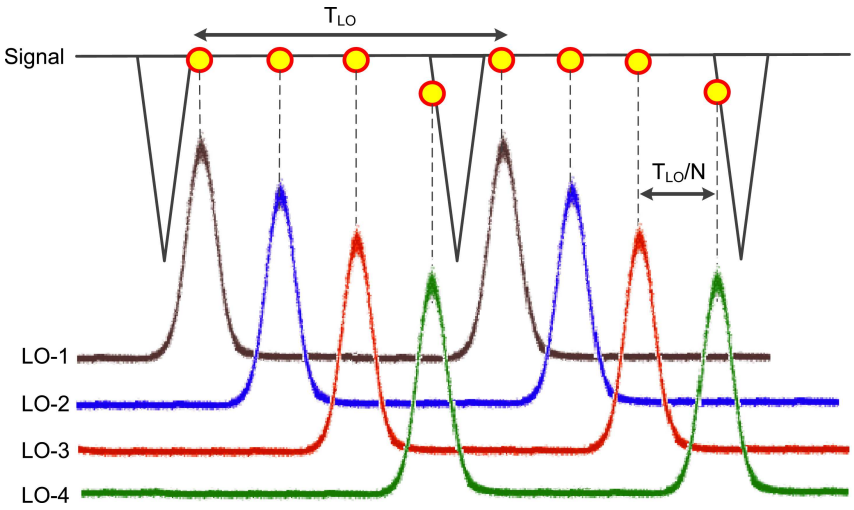

Figure 4.2: Basic idea of equidistance parallel sampling, here with N = 4.

$$t_{i,k} = \tau_i + kT_{\mathrm{LO}}, \qquad k = 0, 1, 2, 3.... \tag{4.2}$$

The ADC sampling is then followed by various stages of digital signal processing to recover and track the phase as well as impairment compensation [12, 46]. Note that the sampling can be done synchronously with one sampling pulse per symbol slot. If the sampled signal with a bandwidth of B_{el} is to be reconstructed without aliasing the required sampling rate of the ADC for a normal coherent receiver is according to the Nyquist Theorem [47]

$$f_{s,\mathrm{el}} = 2B_{\mathrm{s}}, \tag{4.3}$$

where the bandwidth B_{s} is assumed to have a rectangular transfer function. If a parallel optical coherent systems is used instead the required sample rate per ADC will be

$$f_{s,\mathrm{el}} = \frac{2B_{\mathrm{s}}}{N}, \tag{4.4}$$

where N is the number of parallel branches as seen in figure 4.1. As seen the required sample rate per ADC is reduced. This relation is shown in figure 4.3, as seen N = 2 and N = 4 greatly reduces the required ADC sampling rate for this bandwidth span compared to the standard coherent case [12].

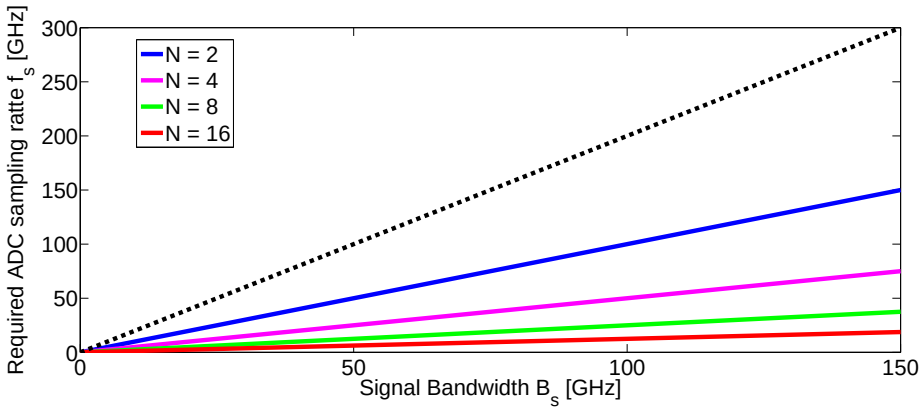

Figure 4.3: Required sampling rate of ADCs as a function of signal bandwidth according to equation 4.4. N is the number of parallel branches. Adapted from [12].

4.1 2-Fold Parallel Optical Sampling

In this project, 2-fold parallel optical sampling was demonstrated. Figure 4.4 shows the basic schematics of a 2-fold parallel optical sampling system. As seen, the pulse train is delayed by a half bit slot so that if the two pulse trains would be combined again the pulses would be placed equidistance with a double repetition rate. The 90° optical hybrids and balanced detectors were integrated in one coherent receiver circuit which was used.

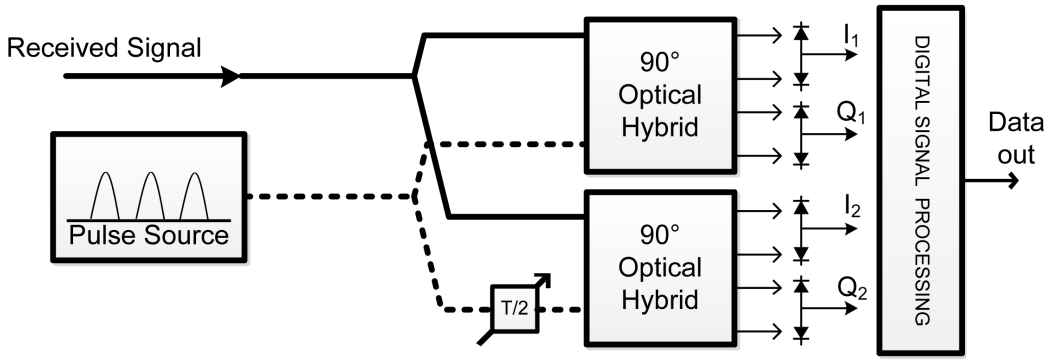

Figure 4.4: Schematics for the basic principle of 2-fold parallel optical sampling.

4.2 Bandwidth Limitation of ADC

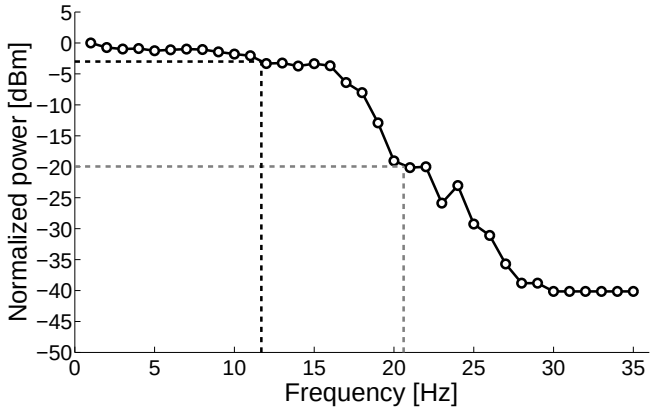

Figure 4.5: Normalized frequency response of one ADC. Black dashed line shows the 3 dB bandwidth at 16 GHz and grey dashed line shows the 20 dB bandwidth at 21 GHz

The frequency response for one of the ADC of the sampling oscilloscope is shown in figure 4.5, the other three ADCs have similar frequency responses. The 3 dB bandwidth can be seen at 16 GHz and at 21 GHz the power has dropped by -20 dB. It should also be noted that at 25 GHz the power has dropped by roughly -27 dB. This measurement was only carried out for one of the four ADCs but no significant difference in frequency response between the different ADCs is expected.

4.3 Experimental Transmitter Configuration

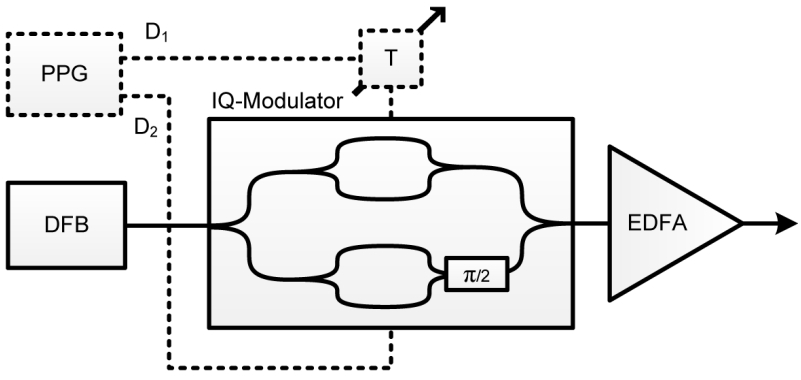

Figure 4.6: Experimental setup of the transmitter, dashed lines indicates components in the electrical domain.

The schematics for the experimental transmitter setup can be seen in figure 4.6. As seen, a distributed feedback laser (DFB) followed by an IQ-modulator was used. The IQ modulator consists of two branches with one MZM in each branch. One of the branches is delayed in such a way that a 90° phase shift is induced and thus the two branches corresponds to the I and Q channel expressed in equation 2.5. The two Mach-Zehnder (MZ) modulators are driven by a pattern generator which generates the output bit streams D_1 and D_2 which in this project were varied between different pseudo-random binary sequence (PRBS) patterns. For the results presented in this project, PRBS of length $2^{11} - 1$ was used. A delay of a few bits was inserted in the electrical domain for one of the bit streams to make sure that if D_1 and D_2 have the same PRBS pattern, all transitions can still occur. The IQ-modulator is followed by an EDFA.

4.4 Experimental Receiver Configuration

The outline of the implemented receiver is shown in figure 4.7. The tunable optical filter used was set to a simple band pass filter with 120 GHz 3 dB-bandwidth for a received 50 Gbaud QPSK signal and 60 GHz for a received 25 Gbaud QPSK signal. The coherent module consisted of two 90° optical hybrids and associated balanced detectors. An optical sampling oscilloscope with four ADCs with bandwidths of 16 GHz, described in Section 4.2, was used to sample the electrical signal from the coherent module. The digital signal processing used after sampling are reviewed in Chapter 5.

As seen in figure 4.7, four optical delays were used. For asynchronous sampling, only one delay for the second pulse branch would be necessary to ensure that the pulses are equidistant. However for synchronized sampling with one sample per symbol, four optical delays were required due to the fact that the optical signal path of the four lines, for the received signal and the LO, were of different lengths. This implies that the signal and pulses will arrive at the coherent module with different relative delays. Further more, the sampling instants of the ADC were all synchronized, i.e. the ADCs sample at

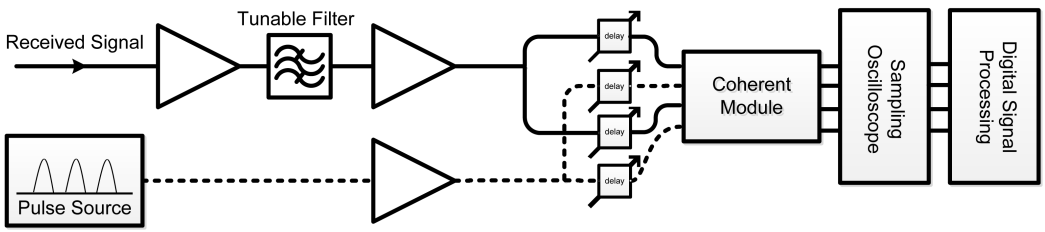

Figure 4.7: Experimental setup for the 2-fold parallel coherent receiver. The coherent module consists of 90° hybrids and balanced detectors described in Section 4.1

the same timing instance which means that the signal and LO pulse for one branch has to be delayed with one symbol slot so that two consecutive symbols are sampled in one timing instant.

Not shown in figure 4.7 are the manual polarization controllers that were used for each branch of the signal and LO paths. These were used to parallelize the states of polarization for the signal and LO.

5. Digital Signal Processing

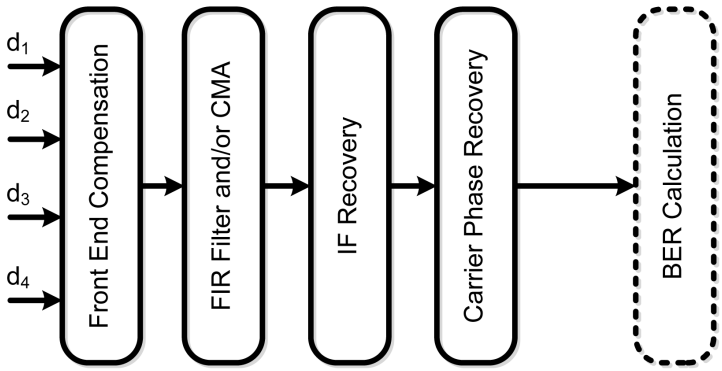

Figure 5.1: Block diagram of the steps included in the digital signal processing.

In this chapter the use and implementation of different steps of digital signal processing will be discussed. The basic block diagram of the digital signal processing from the sampled signals d_1, d_2, d_3 and d_4 to the BER calculation is shown in figure 5.1. The sampled signals are first compensated for having different mean powers from the fact that the gain of the balanced detection and responsivities of the photodetectors and ADCs can be slightly different. The second step is to apply an equalizer using either FIR filtering, CMA or the combination of the two to compensate for linear impairments and ISI caused by the bandwidth limitations of the ADCs. The next step is to recover the intermediate frequency followed by the recovery of the carrier phase to down-convert the signal and to track the phase noise of the LO laser.

5.1 Front End Compensation

The first step of the digital signal processing is to compensate for different responsivities of the photodetectors and the ADCs as well as different gain of the balanced detection. This is often called *front end compensation* and is a quite simple method. Considered the sampled data d_1, d_2, d_3 and d_4 and that data is sampled in such a way that d_1 and d_2 are sampled from the output of one balanced receiver and d_3 and d_4 from the second balanced receiver.

The aim is to normalize the mean power between the two sampled couples. This is done by calculating the scaling factor according to

$$F_{1,2} = \frac{\langle |d_1|^2 \rangle}{\langle |d_2|^2 \rangle}, \qquad F_{3,4} = \frac{\langle |d_3|^2 \rangle}{\langle |d_4|^2 \rangle}, \tag{5.1}$$

where $\langle \cdot \rangle$ denotes the mean value. The scale factor can then be used to make sure that the mean power level is equal by taking for instance $d_2' = d_2 \cdot F_{1,2}$ and $d_4' = d_3 \cdot F_{1,2}$.

5.2 FIR Filter Equalizer

As seen in section 4.2, the system is bandwidth limited at roughly 16 GHz. This will give to rise *ringing* if the signal bandwidth is larger than 16 GHz which in turn can cause ISI. The ringing phenomenon was especially noticeable when a pulse repetition rate of 25 GHz was used. To compensate for this limitation an equalizer is typically implemented. In this project the equalization was done using an finite impulse-response (FIR) filter, using the constant modulus algorithm (CMA) or the combination of both. In this section an equalizer based on FIR filtering is discussed. If $d(n)$ is the received samples from one of the four ADCs the filtered samples $y(n)$ are given by

$$y(n) = d(n) + \sum_{i=1}^{N} c_i d(n-i), \tag{5.2}$$

where N is the number of filter taps and c_i is the i:th filter coefficient [48]. With an adequate number of filter taps and optimized filter coefficient such an equalizer should be able to compensate for the linear effects from bandwidth limited ADCs [49].

The most straight forward method to find the filter coefficients would be to sample a short pulse with low repetition rate to find the impulse response and then optimize the filter coefficients so that the ringing is maximally suppressed. However, since balanced detectors were used, sending a short pulse beating with a CW LO results in no output. Therefore a different method to find the optimum filter coefficients had to be implemented.

5.2.1 FIR Filter Equalizer Optimization Using Steepest Descent Method With Adaptive Step Size

Some assumptions had to be made in order to simplify the implementation of the algorithm. First, the noise is assumed to be independent and have zero mean for sufficiently long data streams. Second, the sampled data of each of the four ADC channels are assumed to be independent. To optimize the FIR filter coefficients, 25 Gbaud QPSK data was transmitted and optically sampled using pulses with a repetition rate of 25 GHz. The sample rate of the

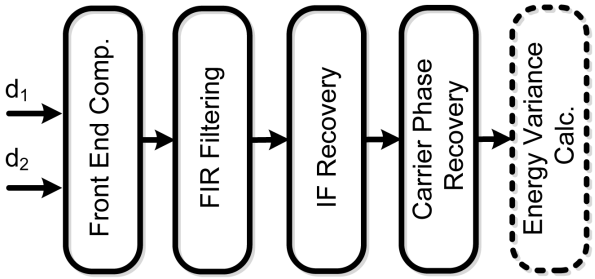

Figure 5.2: Flow diagram of processes from FIR filtering to calculation of energy variance. d1 and d2 are sampled QPSK data of the I and Q channel with known patterns.

ADC was also 25 GHz, i.e. one sample per symbol slot. The system was then optimized so that all sampling instants could be considered to be at optimum and so that the optical signal to noise ratio (OSNR) of the system was high.

To find a measure of quality of the sampled QPSK data a known pattern is transmitted, in this case PRBS pattern with a length of $2^7 - 1$. The data is constructed such that $E = d_1 + jd_2$ where d_1 and d_2 both are known PRBS patterns. The energy variance is then found by the following sum

$$\sigma_{\mathrm{E}} = \sum_{i=1}^{L} \frac{(d_i - \mathbb{E}[d_i])^2}{L}, \tag{5.3}$$

where L is the length of the captured data, $\mathbb{E}[d_i]$ is the expected value of sample i and d_i is the sampled value. The sampled data is normalized such that $\mathbb{E}[|E_i|] = 1$, which means that the expected value of d_i is either of $\pm\sqrt{2}$.

To optimize the filter coefficients the method of steepest descent with respect to the energy variance σ_{E} is used. The filter coefficients, here denoted $\mathbf{c} = [c_1\ c_2\ ...\ c_{N-1}\ c_N]$, is initialized at $\mathbf{c} = 0$ and the energy variance $\sigma_{\mathrm{E}}(\mathbf{c})$ is considered to be a function of the filter coefficients $\mathbf{c}$ such that the σ_{E} is calculated after filtering according to equation 5.2 has been done. It should be noted that both IF recovery and phase estimation is performed before the energy variance is calculated, as seen in the flow diagram in figure 5.2. The filter coefficients $\mathbf{c}$ are optimized iterating the following equation

$$\mathbf{c}_i = \mathbf{c}_c - \mu \bigtriangledown \sigma_{\mathrm{E}}(\mathbf{c}_c), \tag{5.4}$$

where μ is the step size and $\bigtriangledown\sigma_{\mathrm{E}}(\mathbf{c}_c)$ is the steepest descent direction of the energy variance as a function of the filter coefficients. $\mathbf{c}_i$ is the iterated version of the current filter tap vector $\mathbf{c}_c$ [50]. To simplify the implementation, the gradient is only taken in directions such that only one of the filter taps of $\mathbf{c}$ is varied at the same time. This is then iterated until convergence, i.e. when changing any of the filter taps of $\mathbf{c}$ with $\pm\mu$ does not decrease the energy variance σ_{E}.

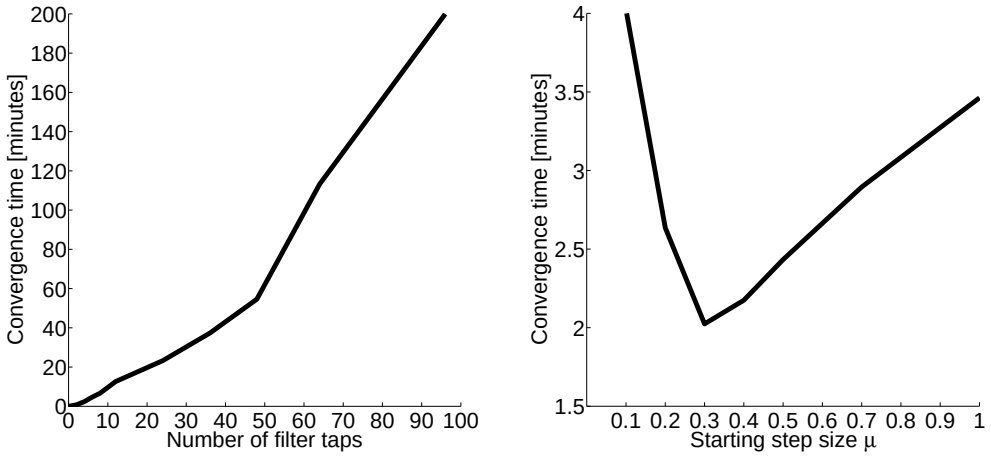

(a) Convergence time with number of filter taps varied.

(b) Convergence time with starting step size varied.

Figure 5.3: Convergence times for the FIR filter tap optimization, using 50000 samples.

To ensure that the algorithm does not converge at a local minima the step size μ is made adaptive. When convergence is reached with a certain step size μ, μ is decreased with small intervals down to a certain minimum value $\mu_{\min}$. If further decrease in σ_{E} can be found with the decreased step size the algorithm continues from that found point with the smaller step size. This should ensure convergence to a global minimum if the starting step size is chosen adequately large. If no further decrease of σ_{E} can be achieved even when using $\mu_{\min}$, the filter taps $\mathbf{c}$ are said to be optimized.

5.2.2 FIR Filter Optimization Convergence Time

It should be noted that this algorithm was constructed without any convergence time requirement, it is basically only executed once for each channel to get the optimized filter coefficients. The FIR filtering itself is a close to real time operation. The convergence time with a fixed μ and $\mu_{\min}$ where only the number of filter taps is changed is showed in figure 5.3(a), it should be noted that this is the convergence time for one pair of ADCs and that the number of samples used from each channel is 50000. As seen the relation is fairly linear, it should be noted though that over 20 filter taps is somewhat excess since all taps above the 20th were found to be close to zero and only seamed to vary due to noise.

If the number of filter taps are kept constant, here 4 taps were used, and the starting step size μ is instead varied the convergence time vary as seen in figure 5.3(b). Here it can be seen that there exists a minimum for the convergence time, i.e. there exists an optimum starting step size μ. If the starting step size μ is kept sufficiently large, so that the algorithm does not

accidently converge to a local minima, μ should have no impact on the final optimized filter coefficients.

5.3 Constant Modulus Algorithm

The constant modulus algorithm was introduced by Godard in 1980 [51] and in this section a brief introduction to the algorithm will be given. This section only considers single polarization signals as no polarization multiplexing was used in this project. Let E_{in} be either of $E_{\text{in}} = d_1 + jd_2$ or $E_{\text{in}} = d_3 + jd_4$. The objective of the CMA is to compensate for linear impairments by equalization using a set of taps h according to

$$E_{\text{out}}[k] = h^T E_{\text{in}}[k], \tag{5.5}$$

where k is a block of samples with the same length as h. To find the filter taps h, the following cost function should be minimized

$$\epsilon^2 = (1 - |E_{\text{out}}|^2)^2. \tag{5.6}$$

To minimize this function, a stochastic gradient algorithm is often used such as

$$h = h - \frac{\mu}{2}\frac{\partial \epsilon^2}{\partial h^*}, \tag{5.7}$$

where μ is the convergence parameter. The complex conjugate derivative is defined as

$$\frac{\partial}{\partial h^*} = \frac{1}{2}\left(\frac{\partial}{\partial \text{Re}\{h\}} + j\frac{\partial}{\partial \text{Im}\{h\}}\right), \tag{5.8}$$

which will give that the filter taps should be updated according to

$$h_{n+1} = h_n + \mu\epsilon E_{\text{in}} E^*_{\text{out,n}}, \tag{5.9}$$

for the n:th iteration [52, 53]. In this project, synchronous sampling with one sample per symbol has been used, i.e. no over-sampling is conducted. This means that for CMA to work properly, the synchronous sampling has to be performed at the optimum sampling instance. However, if the signal would be over-sampled, CMA could be performed on the reconstructed signal. CMA also works for polarization multiplexed signals [52]. For a more profound review of CMA see for instance [53] or [52].

5.4 IF Recovery

The IF is simply recovered by finding the peak in the spectrum of E^4, where E is the sampled field envelope of a QPSK signal. This simple method might be inaccurate if the number of sampled points are too few, which means a low resolution in frequency domain [52]. However, this method worked sufficiently well for this project.

5.5 Carrier Phase Recovery

The LO laser will have a certain phase noise that will distort the detected signal which can be seen as rotation in the constellation diagram. This phase noise needs to be tracked in order to recover the transmitted data [54]. The carrier phase recovery algorithm is based on the *Viterbi and Viterbi* estimator [55] combined with the basic idea that the phase is approximately constant over a small block of samples. The phase estimator for one block is given by

$$\hat{\theta}_b = \frac{1}{4} \arg \left\{ \sum_{l=m_b}^{m_b+M-1} i_l^4 \right\}, \tag{5.10}$$

where M is the block length, m_b is the starting index of block number b and i is the complex photocurrent [55, 52]. However, since the argument function only gives values between $-\pi$ and π, the phase estimate needs to be unwrapped. Without unwrapping, the phase estimation will be limited by $-\pi/4$ and $\pi/4$ which can not track a continuously evolving phase [56, 57]. The basic idea of unwrapping is to ensure that all phase drifts can be tracked, if the tracked phase angle crosses the negative real axis the tracked phase angle should be increased or decreased by 2π [57]. However, even with the use of unwrapping, *cycle slips* can occur, which means that phase noise can cause the phase tracking to "slip" from one stable operation point to another adjacent operation point [58]. The phenomenon of cycle slip will have a major impact on the performance of the system [56].

For a more in-depth review of phase tracking and unwrapping see the classic *Viterbi and Viterbi* paper [55] combined with for instance [56], [57] or [54].

6. Results

In this section the results from the different experimental setups will be presented. All measurements are performed with a back-to-back configuration. The theoretical BER values were derived from [59].

6.1 25 Gbaud QPSK, Back-to-Back Configuration

Figure 6.1 shows the BER performance for 25 Gbaud QPSK signal synchronously sampled with an 8.4 ps optical pulse with one sample per symbol. From figure 6.2 the difference in BER performance from using only FIR filtering, only CMA or the combination of the two can be seen. 25 Gbaud QPSK data sampled with CW LO instead of pulses is also plotted. For this case it is clear that the combination of FIR and CMA gives the best performance. From figure 6.1 it can be seen that the required OSNR for a BER of 10^{-3} is roughly 12.7 dB for the best configuration. It is also seen that the penalty from the theoretical limit is roughly 2.8 dB which is most likely due to imperfections of the optical pulses such as amplitude noise. From figure 6.2, it can be seen that a penalty of roughly 0.8 dB is observed by using a pulsed LO compared to a CW LO. Both these numbers are measured at BER = 10^{-3}.

Figure 6.3 shows the corresponding constellation diagram plotted at a OSNR of 13 dB which roughly corresponds to a BER of 10^{-3} for the best case, i.e. when both FIR filter and CMA were implemented.

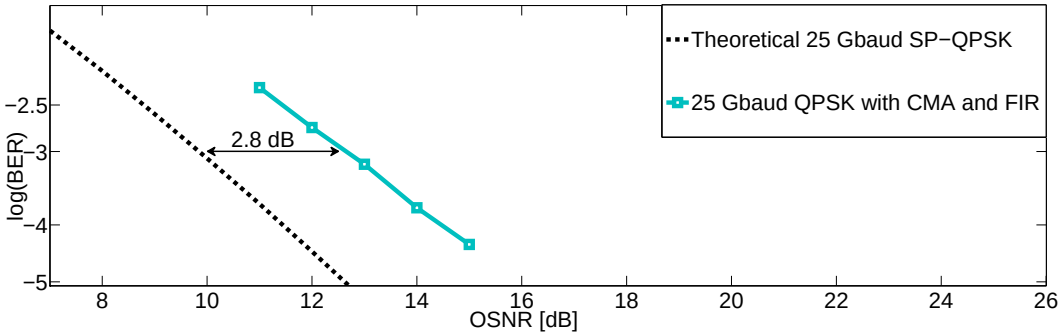

Figure 6.1: Experimental results for 25 Gbaud QPSK data sampled with the 8.4 ps pulse seen in figure 3.5.

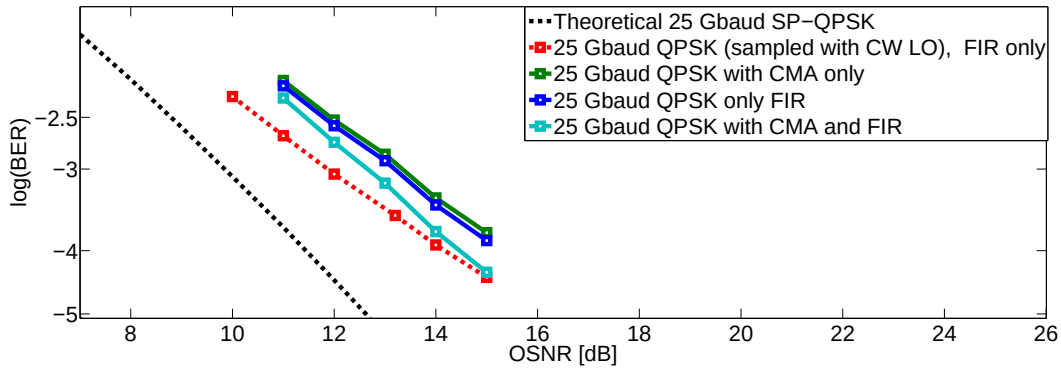

Figure 6.2: Comparison between using FIR filter and CMA in the digital signal processing, same data has been used for the three cases. The red dotted line shows 25 Gbaud QPSK sampled with CW LO.

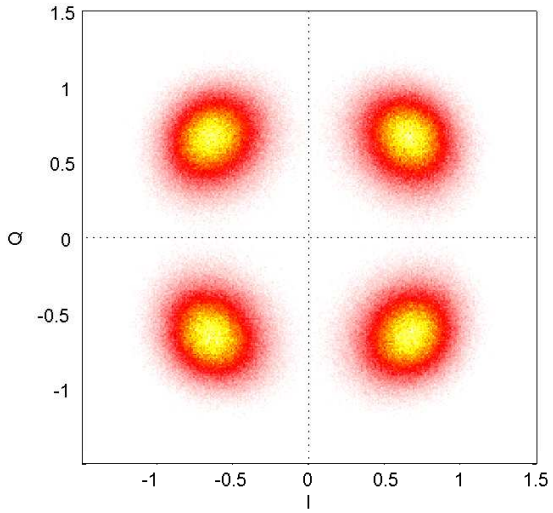

Figure 6.3: Constellation diagram for 25 Gbaud QPSK data sampled with the 8.4 ps pulse seen in figure 3.5 with an OSNR of 13 dB which roughly corresponds to a BER of 10^{-3}.

6.2 50 Gbaud QPSK, Back-to-Back Configuration

Figure 6.4 shows the BER performance for 50 Gbaud QPSK signal sampled with an 8.4 ps pulse with one sample per symbol synchronously sampled. Note that the measurement is performed with a back-to-back configuration and that only one of the parallel branches was sampled, i.e. only every second symbol slot is sampled. The reason for this was unavailability of the number of optical delays that were needed during the time frame of this project. However, there is no significant difference seen if switched to the second parallel branch. From figure 6.5 the difference in BER performance from using only FIR filtering, only CMA or the combination of the two can be seen. Note that no plot of 50 Gbaud QPSK data sampled with CW LO is shown with the simple reason that the BER for this measurement was too high to measure. For this case, the combination of FIR filtering and CMA and the use of only CMA seems to give similar results while implementing only FIR filter gives a worse result. From figure 6.4 it can be seen that the required OSNR for a BER of 10^{-3} is roughly 15.4 dB for the best configuration. It is also seen that the penalty from the theoretical limit is roughly 2.6 dB which is similar to the 25 Gbaud QPSK case measured at BER = 10^{-3}.

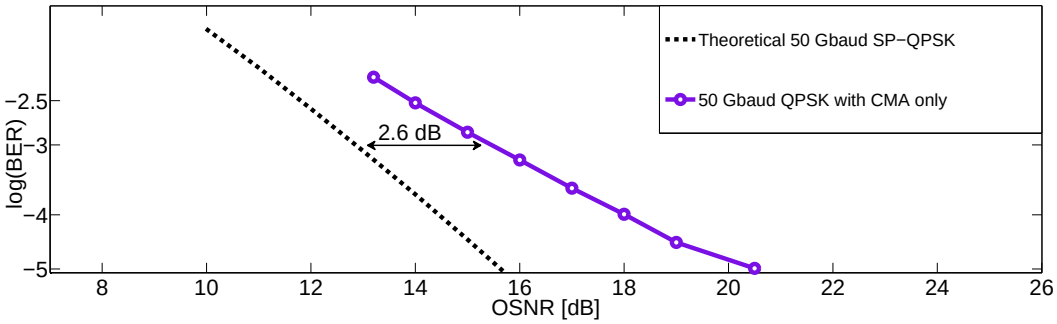

Figure 6.4: Experimental results for 50 Gbaud QPSK data sampled with the 8.4 ps pulse seen in figure 3.5

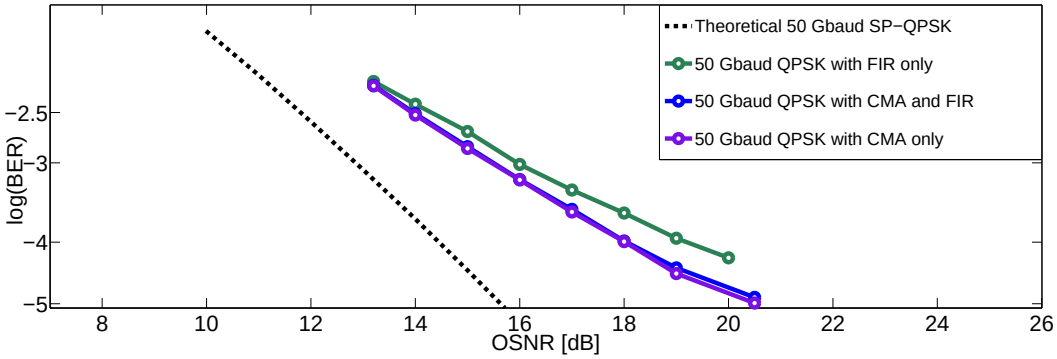

Figure 6.5: Comparison between using FIR filter and CMA in the digital signal processing for sampled 50 Gbaud QPSK signals. Same data has been used for the three cases.

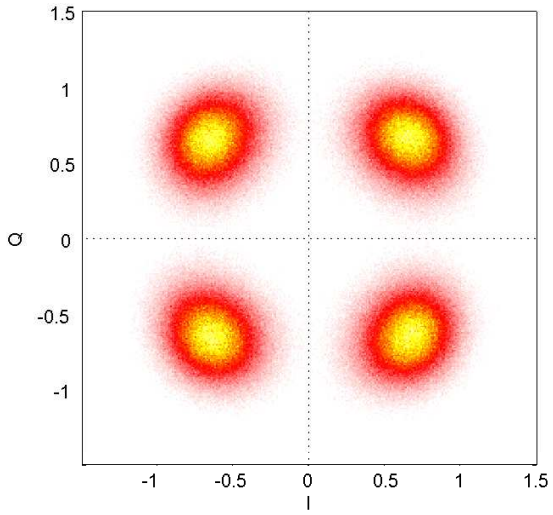

Figure 6.6: Constellation diagram for 50 Gbaud QPSK data sampled with the 8.4 ps pulse seen in figure 3.5 with an OSNR of 16 dB which roughly corresponds to a BER of 10^{-3}.

6.3 Asynchronous Sampling, Back-to-Back Configuration

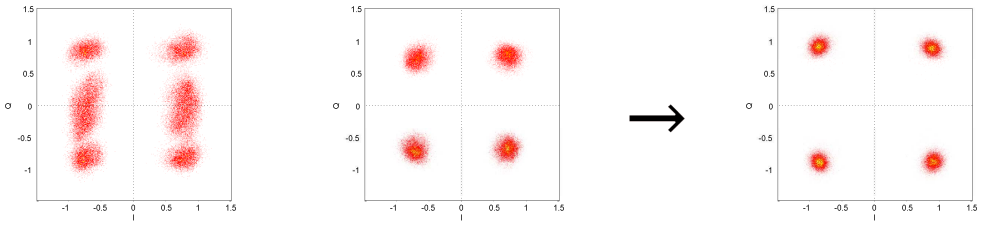

(a) 1th sample (b) 2nd sample (c) After resample and CMA

Figure 6.7: Constellation diagrams showing constellation at the first sample (a) and the second sample (b). (c) shows the constellation diagram after CMA has been applied to the resampled signal.

Note that the main focus of this project was synchronous sampling of QPSK signals with one sample per bit. However some minor experiments on asynchronous sampling were conducted with 12.5 GHz QPSK data and a pulsed LO with 12.5 GHz repetition rate. Figure 6.7(a) and figure 6.7(b) shows the constellation diagrams for where the sampling was done, i.e. in the same fashion as if it would have been one sample per symbol. The two sampling points per symbol are roughly performed as in figure 6.8 where figure 6.7(a) corresponds to the leftmost sampling point in the figure. As seen, this sampling is done at a transition point. Since the sampling is done with 2 samples per symbol slot the Nyquist criterion can be satisfied, see equation 4.3. The signal can then be reconstructed and CMA can be applied to the reconstructed signal. The constellation diagram after such operations is shown in figure 6.7(c). Note that this result is obtained at the best OSNR that could be achieved.

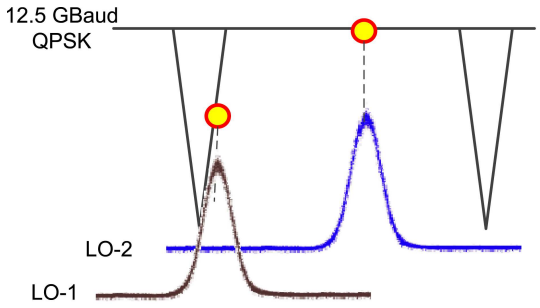

Figure 6.8: Visualization of how the asynchronous sampling in figure 6.7 is done.

7. Conclusions

A real-time parallel optical sampling receiver has been demonstrated for detection of single polarization QPSK signals with synchronous sampling with one sample per symbol slot. The QPSK signal was sampled in the optical domain by an 8.4 ps optical pulse generated by a pulse source consisting of two MZ-modulators to generate a pulse train and a phase modulator to induce chirp on the pulses. The pulse train was then propagated through a dispersive medium to achieve compression to a FWHM of 8.4 ps.

50 Gbaud QPSK signals has been successfully sampled with a BER performance penalty of 2.6 dB at a BER of 10^{-3}. Further, 25 Gbaud QPSK signals has been sampled with a BER performance penalty of 2.8 dB at a BER of 10^{-3}. These BER performance penalties are most likely due to pulse imperfections such as amplitude noise.

Furthermore, the performance difference of applying equalization through CMA and/or FIR filtering to the sampled 25 and 50 Gbaud QPSK signals was investigated. For 50 Gbaud, it was seen that CMA alone could achieve the best BER performance whilst for 25 Gbaud the combination of CMA and FIR filtering gave the best results.

8. Future Directions

First of all, full synchronous sampling with one sample per symbol slot for 50 Gbaud QPSK data should be demonstrated so that the performance of a fully functional sampling system can be measured. The measurements of 50 Gbaud QPSK in this project was only sampled with one of the 2-fold parallel branches. This was due to that certain equipments were unavailable during the time frame of this project. However, no significant difference in performance is expected since the schematics of the two branches are identical.

Furthermore, it would be interesting to perform the same measurements over transmission links of fiber to compare with the back-to-back performance measured in this project.

Moreover, a modification of the current system to support asynchronized sampling with two samples per symbols for up to 50 Gbaud QPSK signals would be of great interest. With such a system, the signal can be reconstructed and important features such as transitions can be investigated and re-sampling at the optimum sampling instance can be performed. Furthermore, digital dispersion compensation can be implemented for such a system which for example was shown in [12].

It would also be interesting to investigate the systems performance on other formats than NRZ-QPSK which was used throughout this project. For example RZ-QPSK, 16-QAM or 8-PSK could be studied.

A very interesting development of the current system would be to expand the system to 4-fold sampling. For this an additional of 4 ADCs and another coherent module would be required. Additional 4 ADCs could be obtained by using another oscilloscope of the same type used in this project, this however is a major investment. The use of 4-fold sampling would allow for example synchronous sampling of 100 Gbaud data with one sample per slot, synchronous sampling of polarization multiplexed 50 Gbaud data with one sample per slot or asynchronous sampling of 50 Gbaud data with two samples per symbol. However, problems with synchronization between two sampling oscilloscopes can occur which was reported in [12].

A more profound study of how different features of the sampling pulses impact the receiver is needed. The sampling of 50 Gbaud QPSK signals suffered a penalty of 2.6 dB from the theoretical value at BER of 10^{-3} which was most likely due to pulse imperfections. As for now it is clear that the pulse characteristics has a strong impact on the performance, for example a

too narrow pulse caused the sampling of 50 Gbaud QPSK to suffer from a lot of errors. However, if the pulse source was built with a repetition rate of 12.5 GHz instead of 25 GHz, very narrow pulses seamed to affect the performance less. One possible reason could be that to much of the power contained in a narrow pulse was cut away due to the bandwidth limitation. However, more features of the pulse than just the pulse width and spectrum width should be investigated. Suggestions of such features are amplitude SNR, timing jitter, residual chirp, pedestal, extinction ration and pulse symmetry.

References

[1] T. H. Maiman, "Stimulated optical radiation in ruby masers," *Nature*, vol. 187, p. 493, 1960.

[2] K. Kao and G. A. Hockham, "Dielectric-fibre surface waveguides for optical frequencies," *PROC. IEE*, vol. 113, no. 7, pp. 1151–1158, 1966.

[3] F. P. Kapron, D. B. Keck, and R. D. Maurer, "Radiation losses in glass optical waveguides," *Applied Physics Letters*, vol. 17, pp. 423–425, Nov 1970.

[4] J. Zyskind and A. Srivastava, *Optically Amplified WDM Networks*, pp. 68–70. Academic Press, Elsevier Science & Technology, 2009.

[5] K. Nagayama, M. Kakui, M. Matsui, I. Saitoh, and Y. Chigusa, "Ultra-low-loss (0.1484 dB/km) pure silica core fibre and extension of transmission distance," *Electronics Letters*, vol. 38, pp. 1168–1169, Sep 2002.

[6] S. Poole, D. Payne, R. Mears, M. Fermann, and R. Laming, "Fabrication and characterization of low-loss optical fibers containing rare-earth ions," *Lightwave Technology, Journal of*, vol. 4, pp. 870–876, Jul 1986.

[7] M. Sköld, *Signal Characterization in Optical Networks*. PhD thesis, Chalmers University of Technology, 2008.

[8] G. Agrawal, *Lightwave Technology: Telecommunication Systems*. Wiley-Interscience, 2nd ed., 2005.

[9] E. Tipsuwannakul, *Transmission of Multi-level DPSK Signals in Optical Systems*. Licentiate thesis, Chalmers University of Technology, 2010.

[10] M. Sjödin, *Self-Homodyne Coherent Systems using Advanced Modulation Formats*. Licentiate thesis, Chalmers University of Technology, 2010.

[11] Tektronix, Inc., *Digital and Mixed Signal Oscilloscopes DPO/DSA/MSO70000 Series Data Sheet*, Jul 2011.

[12] J. Fischer, R. Ludwig, L. Molle, C. Schmidt-Langhorst, C. Leonhardt, A. Matiss, and C. Schubert, "High-speed digital coherent receiver based on parallel optical sampling," *Lightwave Technology, Journal of*, vol. 29, pp. 378–385, Feb 2011.

[13] K. Okamoto and F. Ito, "Dual-channel linear optical sampling for simultaneously monitoring ultrafast intensity and phase modulation," *Lightwave Technology, Journal of*, vol. 27, pp. 2169–2175, Jun 2009.

[14] J. Anderson, *Digital Transmission Engineering*, pp. 43–63 and 79–85. IEEE Series on Digital & Mobile Communication, IEEE Press, 2nd ed., 2005.

[15] H. Sasaoka, *Mobile Communications*, pp. 89–92. Wave summit course, Ohmsha, 2000.

[16] K. Wesolowski, *Introduction to Digital Communication Systems*, pp. 254–271. John Wiley & Sons, 2009.

[17] J. Anderson, *Digital Transmission Engineering*. IEEE Series on Digital & Mobile Communication, IEEE Press, 2nd ed., 2005.

[18] G. Agrawal, *Lightwave Technology: Telecommunication Systems*, pp. 26–32. Wiley-Interscience, 2nd ed., 2005.

[19] P. Winterling, *Optical Modulation Methods*. White paper, JDS Uniphase, 2008.

[20] R. Freund, D.-D. Gross, M. Seimetz, L. Molle, and C. Caspar, "30 Gbit/s RZ-8-PSK transmission over 2800 km standard single mode fibre without inline dispersion compensation," *Optical Fiber communication/National Fiber Optic Engineers Conference*, pp. 1–3, 2008.

[21] Y. Mori, C. Zhang, M. Usui, K. Igarashi, K. Katoh, and K. Kikuchi, "200-km transmission of 100-Gbit/s 32-QAM dual-polarization signals using a digital coherent receiver," *Optical Communication, 2009. ECOC '09. 35th European Conference on*, 2009.

[22] A. Sano, T. Kobayashi, A. Matsuura, S. Yamamoto, S. Yamanaka, E. Yoshida, Y. Miyamoto, M. Matsui, M. Mizoguchi, and T. Mizuno, "100 120-Gb/s PDM 64-QAM transmission over 160 km using linewidth-tolerant pilotless digital coherent detection," *Optical Communication (ECOC), 2010 36th European Conference and Exhibition on*, 2010.

[23] S. Okamoto, T. Omiya, K. Kasai, M. Yoshida, and M. Nakazawa, "140 Gbit/s coherent optical transmission over 150 km with a 10 Gsymbol/s polarization-multiplexed 128 QAM signal," *Optical Fiber Communication (OFC), collocated National Fiber Optic Engineers Conference, 2010 Conference on (OFC/NFOEC)*, 2010.

[24] M. Nakazawa, S. Okamoto, T. Omiya, K. Kasai, and M. Yoshida, "256 QAM (64 Gbit/s) coherent optical transmission over 160 km with an optical bandwidth of 5.4 GHz," *Optical Fiber Communication (OFC),*

collocated National Fiber Optic Engineers Conference, 2010 Conference on (OFC/NFOEC), 2010.

[25] S. Okamoto, K. Toyoda, T. Omiya, K. Kasai, M. Yoshida, and M. Nakazawa, "512 QAM (54 Gbit/s) coherent optical transmission over 150 km with an optical bandwidth of 4.1 GHz," *Optical Communication (ECOC), 2010 36th European Conference and Exhibition on*, 2010.

[26] M. Seimetz, *High-Order Modulation for Optical Fiber Transmission*, pp. 79–85. Springer Series in Optical Sciences, Springer, 2009.

[27] I. Kaminow, T. Li, and A. Willner, *Optical Fiber Telecommunications 5*, pp. 95–129. No. 1 in Optics and Photonics, Academic Press, 2008.

[28] R. Mears, L. Reekie, I. Jauncey, and D. Payne, "Low-noise erbium-doped fibre amplifier operating at 1.54 μm," *Electronics Letters*, vol. 23, pp. 1026–1028, Oct 1987.

[29] K. Ho, *Phase-Modulated Optical Communication Systems*, pp. 61–66. Springer, 2005.

[30] A. Wiberg, C.-S. Bres, B. Kuo, J. Zhao, N. Alic, and S. Radic, "Pedestal-free pulse source for high data rate optical time-division multiplexing based on fiber-optical parametric processes," *Quantum Electronics, IEEE Journal of*, vol. 45, pp. 1325–1330, Nov 2009.

[31] J. Fischer, R. Ludwig, L. Molle, C. Schmidt-Langhorst, C. Leonhardt, A. Matiss, and C. Schubert, "Digital coherent receiver based on parallel optical sampling," in *Optical Communication (ECOC), 2010 36th European Conference and Exhibition on*, pp. 1–3, Sep 2010.

[32] K. Igarashi, K. Katoh, K. Kikuchi, K. Imai, and M. Kourogi, "Generation of 10-GHz 2-ps optical pulse train over the C band based on an optical comb generator and its application to 160-Gbit/s OTDM systems," in *Optical Communication, 2008. ECOC 2008. 34th European Conference on*, pp. 1–2, Sep 2008.

[33] C. Dorrer, C. Doerr, I. Kang, R. Ryf, J. Leuthold, and P. Winzer, "Measurement of eye diagrams and constellation diagrams of optical sources using linear optics and waveguide technology," *Lightwave Technology, Journal of*, vol. 23, pp. 178–186, Jan 2005.

[34] J. Li, P. Andrekson, and B. Bakhshi, "Direct generation of subpicosecond chirp-free pulses at 10 GHz from a nonpolarization maintaining actively mode-locked fiber ring laser," *Photonics Technology Letters, IEEE*, vol. 12, pp. 1150–1152, Sep 2000.

[35] B. Bakhshi and P. Andrekson, "40 GHz actively modelocked polarisation maintaining erbium fibre ring laser," *Electronics Letters*, vol. 36, pp. 411–413, Mar 2000.

[36] E. Yoshida, Y. Kimura, and M. Nakazawa, "20 GHz, 1.8 ps pulse generation from a regeneratively modelocked erbium-doped fibre laser and its femtosecond pulse compression," *Electronics Letters*, vol. 31, pp. 377–378, Mar 1995.

[37] K. Igarashi, K. Katoh, and K. Kikuchi, "Generation of 10-GHz, 2-ps optical pulse train with high extinction ratio and low timing jitter from a continuous wave tunable over the entire C band," in *Optical Communication, 2005. ECOC 2005. 31st European Conference on*, vol. 1, pp. 39–40, Sep 2005.

[38] H. Hu, J. Yu, L. Zhang, A. Zhang, Y. Li, Y. Jiang, and E. Yang, "Pulse source based on directly modulated laser and phase modulator," *Opt. Express*, vol. 15, pp. 8931–8937, Jul 2007.

[39] T. Komukai, T. Yamamoto, and S. Kawanishi, "Optical pulse generator using phase modulator and linearly chirped fiber bragg gratings," *Photonics Technology Letters, IEEE*, vol. 17, pp. 1746–1748, Aug 2005.

[40] E. Swanson and S. Chinn, "23-GHz and 123-GHz soliton pulse generation using two CW lasers and standard single-mode fiber," *Photonics Technology Letters, IEEE*, vol. 6, pp. 796–798, Jul 1994.

[41] M. Sköld, M. Westlund, H. Sunnerud, and P. A. Andrekson, "All-optical waveform sampling in high-speed optical communication systems using advanced modulation formats," *J. Lightwave Technol.*, vol. 27, pp. 3662–3671, Aug 2009.

[42] T. Sakamoto, T. Kawanishi, M. Tsuchiya, and M. Izutsu, "Picosecond pulse generation with a single-stage standard Mach-Zehnder modulator employed," in *Optical Communications, 2006. ECOC 2006. European Conference on*, pp. 1–2, Sep 2006.

[43] J. Fischer, R. Ludwig, L. Molle, C. Schmidt-Langhorst, A. Galperin, T. Richter, C. Leonhardt, A. Matiss, and C. Schubert, "High-speed digital coherent receiver with parallel optical sampling," in *Optical Fiber Communication (OFC), collocated National Fiber Optic Engineers Conference, 2010 Conference on (OFC/NFOEC)*, pp. 1–3, Mar 2010.

[44] M. Sköld, M. Westlund, H. Sunnerud, and P. Andrekson, "All-optical waveform sampling in high-speed optical communication systems using advanced modulation formats," *Lightwave Technology, Journal of*, vol. 27, pp. 3662–3671, Aug 2009.

[45] G. Agrawal, *Nonlinear Fiber Optics*, pp. 69–72. Academic Press, 2007.

[46] X. Chen, X. Xie, I. Kim, G. Li, H. Zhang, and B. Zhou, "Coherent detection using optical time-domain sampling," *Photonics Technology Letters, IEEE*, vol. 21, pp. 286–288, Mar 2009.

[47] H. Nyquist, "Certain topics in telegraph transmission theory," *American Institute of Electrical Engineers, Transactions of the*, vol. 47, pp. 617–644, Apr 1928.

[48] B. Mulgrew, P. Grant, and J. Thompson, *Digital Signal Processing: Concepts and Applications*, pp. 153–182. Palgrave Macmillan, 2nd ed., 2003.

[49] M. Nakazawa, K. Kikuchi, and T. Miyazaki, *High Spectral Density Optical Communication Technologies*, pp. 40–42. Optical and Fiber Communications Reports, Springer, 2010.

[50] C. Kelley, *Iterative Methods for Optimization*, pp. 39–40. Frontiers in applied mathematics, SIAM, 1999.

[51] D. Godard, "Self-recovering equalization and carrier tracking in two-dimensional data communication systems," *Communications, IEEE Transactions on*, vol. 28, pp. 1867–1875, Nov 1980.

[52] S. Savory, "Digital coherent optical receivers: Algorithms and subsystems," *Selected Topics in Quantum Electronics, IEEE Journal of*, vol. 16, pp. 1164–1179, Sep-Oct 2010.

[53] P. Johannisson, H. Wymeersch, M. Sjödin, A. Tan, E. Agrell, P. Andrekson, and M. Karlsson, "Convergence comparison of the CMA and ICA for blind polarization demultiplexing," *Optical Communications and Networking, IEEE/OSA Journal of*, vol. 3, pp. 493–501, Jun 2011.

[54] M. Seimetz, *High-Order Modulation for Optical Fiber Transmission*, pp. 94–110. Springer Series in Optical Sciences, Springer, 2009.

[55] A. Viterbi and A. Viterbi, "Nonlinear estimation of psk-modulated carrier phase with application to burst digital transmission," *Information Theory, IEEE Transactions on*, vol. 29, pp. 543–551, Jul 1983.

[56] E. Ip and J. Kahn, "Feedforward carrier recovery for coherent optical communications," *Lightwave Technology, Journal of*, vol. 25, pp. 2675–2692, Sep 2007.

[57] M. Taylor, "Phase estimation methods for optical coherent detection using digital signal processing," *Lightwave Technology, Journal of*, vol. 27, pp. 901–914, Apr 2009.

[58] G. De Jonghe and M. Moeneclaey, "Cycle slip analysis of the NDA FF carrier synchronizer based on the Viterbi and Viterbi algorithm," in *Communications, 1994. ICC '94, SUPERCOMM/ICC '94, Conference Record, 'Serving Humanity Through Communications.' IEEE International Conference on*, vol. 2, pp. 880–884, May 1994.

[59] J. Proakis and M. Salehi, *Digital Communications*. McGraw-Hill Higher Education, McGraw-Hill, 4th ed., 2001.